A Thesis of the Master's Degree

Findings of Ultrasonography and Magnetic Resonance Imaging in the Animal model of Cholangiocarcinoma induced with C. cinensis and N-nitrosodimethylamine

간흡충과 N-nitrosodimethylamine을 이용한 담관암의 동물모델에서의 초음파와 자기공명영상 소견

Feb 2014

The Department of Radiology,
Seoul National University
College of Medicine

Woo Hyunsik

Findings of Ultrasonography and Magnetic Resonance Imaging in the Animal model of Cholangiocarcinoma induced with C. cinensis and N-nitrosodimethylamine

by

Woo Hyunsik

A thesis submitted to the Department of Radiology in partial fulfillment of the requirements for the Degree of Master of Science in Radiology at Seoul National University College of Medicine

Feb 2014

Approved by Thesis Committee:

Professor _____Chairman

Professor _____Vice chairman

Professor _____

초 록

서론: 이 연구의 목적은 간흡충과 N-nitrosodimethylamine (NMDA) 를 이용한 담관암의 동물모델에서의 초음파와 자기공명영상 소견 및 담관암과 전암성 병변의 발견 가능성을 평가하는 것이다.

방법: 24마리의 4-5주령 수컷 시리안 골든 햄스터를 아래와 같이 네 그룹으로 분리하였다.

- 그룹 I (정상군): 5마리
- 그룹 II (CS): 햄스터 한 마리당 30마리의 간흡충을 투여, 5마리
- 그룹 III (NMDA): 12.5ppm 농도의 NMDA 를 포함한 물을 8주간 투여, 5마리
- 그룹 IV (CS+NMDA): 간흡충과 NMDA 를 포함한 물을 투여, 9마리

모든 햄스터에 대해서 투여 전 기저 초음파부터 투여 후 12주까지 2주 간격으로 초음파를 시행하고, 햄스터 희생 전에 조영증강 자기공명영상을 시행하였다. 햄스터 희생 후 적출된 간에 대해 병리조직학적 검사를 시행하고, 영상소견과 병리소견을 비교하였다.

결과: CS+NMDA 그룹에서 6주에 처음 담관암이 발견되었다. 총 12개의 담관암이 병리조직학적으로 확인되었으며, 그 중 10개의 담

관암이 초음파 혹은 자기공명영상에서 발견되었다. 초음파와 자기공명영상 모두 담관주위 염증, 담관 확장, 낭종, 쓸개 내 슬러지 등의 소견을 잘 보여주었다. 담관주위 염증과 담관암 모두 초음파 상에서 고에코, T2 강조 자기공명영상에서 고신호의 병변으로 보였다.

결론: 초음파와 자기공명영상 모두 담관암의 발견에 유용하였다. 전암성 병변의 발견에서 자기공명영상의 유용성을 확인하였으나 T2 강조영상에서의 신호강도는 비특이적이었다. 결론적으로, 담관암 동물모델에서 전암성 병변을 영상의학적으로 발견할 수 있을 것으로 예상되며, 향후 담관암의 전암성 병변의 영상소견을 규명하여 궁극적으로 담관암의 조기발견 및 치료에 기여할 수 있을 것으로 기대된다.

주요어: 담관암, 간흡충, 햄스터, 초음파, 자기공명영상

학 번: 2012-21699

Abstract

Introduction

The purpose of this study is to evaluate image findings and detectability of cholangiocarcinoma (CCA) and its precancerous lesions using in-vivo high-resolution ultrasonography (USG) and magnetic resonance imaging (MRI) enhanced with hepatobiliary-specific contrast media agent in the animal model of CCA using Syrian golden hamsters with C. sinensis and N-Nitrosodimethylamine (NMDA).

Methods

A total of 24 male Syrian golden hamsters (Mesocricetus auratus) of 4-5 weeks old were divided randomly into 4 groups as follows: 5 hamsters of Group I (Control) as an uninfected control, 5 hamsters of Group II (CS) receiving 30 metacercariae of C. sinensis per each hamster, 5 hamsters of Group III (NDMA) receiving NMDA in drinking water, and 9 hamsters of Group IV (CS+NDMA) receiving both metacercariae and NDMA.

USG was performed every other week from baseline to 12th week of infection. MRI was done from 4th week to 12th week prior to sacrifice, followed by histopathologic examination of the liver. Image findings in USG and MRI were analyzed and compared with histopathologic findings.

Results

CCAs appeared in the hamsters of CS+NDMA group as early as 6th

week of infection. There were a total of 12 CCAs and 10 of them were demonstrated by USG or MRI. USG and MRI also showed other findings of disease progression such as periductal increased echogenicity or signal intensity, ductal dilatation, complicated cysts, and sludges in the gallbladder. Both periductal inflammatory change and CCAs appeared as lesions of increased echogenicity on USG and increased signal intensity on T2WI of MRI.

Conclusions

High-resolution USG and MRI are useful to detect the occurrence of CCAs noninvasively. Although USG was determined not to be a suitable modality in monitoring of the early precancerous lesions of CCA, MRI showed some potential to visualize precancerous lesions of CCAs, but the signal intensity on T2WI was nonspecific to distinguish precancerous lesions from periductal inflammatory change or CCAs. MRI of closer interval with more powerful sequences might be able to demonstrate the precancerous lesions of CCAs better.

Keywords: cholangiocarcinoma, clonorchiasis, hamster, ultrasonography, magnetic resonance imaging

Student Number: 2012-21699

Table of Contents

List of Tables

List of Figures

List of Abbreviations

CCA: Cholangiocarcinoma

NMDA: N-nitrosodimethylamine

CS: *Clonorchis cinensis*

USG: Ultrasonography

MRI: Magnetic resonance imaging

TSE: Turbo spin-echo

PACE: prospective acquisition correction

SPAIR: spectral adiabatic inversion recovery

HASTE: half-Fourier acquisition single-shot turbo spin-echo

GRE: gradient-echo

VIBE: volumetric interpolated breath-hold examination

TR: relaxation time

TE: echo time

FA: flip angle

NEX: number of excitation

FOV: field of view

T1WI: T1-weighted image

T2WI: T2-weighted image

H&E: hematoxylin and eosine

LN: lymph node

Introduction

Liver cancer is one of the most common cancers in Southeast Asia and the death rate among Koreans is one of the highest in the world [1]. Among primary liver cancer, cholangiocarcinoma (CCA) is difficult to diagnose and usually fatal because of its late clinical presentation and the lack of effective non-surgical therapeutic modalities. According to a recent study, approximately 10% of CCAs in Korea and 25% of CCAs in endemic Asian countries are caused by chronic infection of *C. sinensis* [2].

There is an established model of CCA using Syrian golden hamsters with *C. sinensis* and sub-carcinogenic level of N-Nitrosodimethylamine (NDMA) [3, 4], which can be found in the diverse consumable items, especially fermented or cured meat, fish, beers, and tobacco smoke [5]. Thus, humans infected with *C. sinensis* are always at risk of developing CCA. Therefore, understanding of carcinogenesis and early findings of CCA in *C. sinensis* infection is essential to improve diagnosis and treatment of CCA.

Early detection and treatment of CCA is crucial to improve prognosis of CCA. As imaging study plays a major role in diagnosis of CCA, understanding of early image findings of CCA and its precancerous lesions is needed for early detection of CCA. In this regard radiologic evaluation of this animal model, where CCAs occur spontaneously, might elucidate the image findings of precancerous lesions of CCA.

For proper understanding of carcinogenesis of CCA, longitudinal analysis of tumor development in animal study would be needed. However,

confirmation of tumor development is not so easy because histopathologic confirmation cannot be done before sacrifice of the animal. In the previous study, serial sacrifices of the animals were done to monitor carcinogenesis of CCA [6]. By virtue of noninvasiveness of in-vivo imaging, longitudinal analysis and monitoring of the progression of CCA can be feasible [7]. Moreover, recent advances in imaging technology such as high-resolution ultrasonography (USG) and magnetic resonance imaging (MRI) will give in-vivo images of better quality than before. Hepatobiliary-specific MRI contrast media agent can improve detection and characterization of various hepatocellular and non-hepatoceullar lesions [8]. These technical advances might demonstrate the development of CCA or precancerous lesions.

The purpose of this study is to evaluate image findings and detectability of CCA and its precancerous lesions using in-vivo high-resolution USG and MRI enhanced with hepatobiliary-specific contrast media agent in the animal model of CCA using Syrian golden hamsters with *C. sinensis* and NMDA. Image findings in USG and MRI were analyzed and compared with histopathologic findings.

Materials and Methods

Approval of the Institutional Animal Care and Use Administrative Committee and Institutional Biosafety Committee of the Seoul National University were obtained. All experiments were in accordance with the general guidelines issued by the National Institutes of the Health for the Care

of Laboratory Animals.

1) Experimental design

Metacercariae were collected from naturally infected freshwater fishes *Pseudorasbora parva*. The fishes were digested with 0.5% pepsin solution with HCl. Metacercariae of *C. sinensis* were isolated under stereomicroscopic identification [9].

A total of 24 male Syrian golden hamsters (Mesocricetus auratus) of 4-5 weeks old were divided randomly into 4 groups as follows: 5 hamsters of **Group I (Control)** as an uninfected control, 5 hamsters of **Group II (CS)** receiving 30 metacercariae of C. sinensis per each hamster, 5 hamsters of **Group III (NDMA)** receiving NMDA in drinking water, and 9 hamsters of **Group IV (CS+NDMA)** receiving both metacercariae and NDMA. Infection of the hamsters with metacercariae was done through intragastric intubation. NMDA was provided to the hamsters in drinking water at a concentration of 12.5 ppm for 8 weeks.

USG was performed every other week from baseline to 12^{th} week of infection. MRI was done from 4^{th} week to 12^{th} week prior to sacrifice, followed by histopathologic examination of the liver. The grouping and experimental design of this study are summarized in **Figure 1**.

2) In-vivo ultrasonography

All hamsters were subjected to abdominal USG every other week

from baseline to 12th week of infection to observe any abnormal findings or changes including echogenicity of the liver, intrahepatic ductal dilatation, lymph node enlargement, hepatic focal lesion or gallbladder lesion. USG was performed subcostally by one radiologist (Woo H) with supine position of the hamsters under general anesthesia. A high-resolution 7-15MHz linear transducer was used (transducer: L15-7io. machine: iU22; Philips Healthcare, Andover, US). A mixture of 10mg/kg of xylazine hydrochloride (Rompun; Bayer, Seoul, Korea) and 30mg/kg of zolazepam (Zoletil; Virbac, Carros, France) were used for anesthesia. The anesthetic solution was injected into the thigh muscle.

3) In-vivo magnetic resonance imaging

Contrast-enhanced MRI was done from 4th week to 12th week prior to sacrifice in order to compare with histopathologic findings. For the hamsters of CS+NMDA group, additional noncontrast MRI was done two weeks before sacrifice. A 3T MR imaging unit (Magnetom Trio; Siemens Medical Solutions, Erlangen, Germany) with an 8-channel animal receiver coil was used. 1.3ml/kg of 0.25mmol/ml solution of gadoxetic acid disodium (Primovist; Bayer Schering Pharma, Berlin, Germany) was used as contrast media. Contrast media was injected directly into the left ventricle in a bolus under the guidance of USG using a 26-gauze needle. MRI was taken with prone position of the hamsters under general anesthesia using the same anesthetic solution used in USG.

Axial T2-weighted TSE (turbo spin-echo) sequence with navigator-triggered PACE (prospective acquisition correction) (TR/TE 7218.8/83.0, FA 140, NEX 2, FOV 80x65mm, matrix 256x177, slice thickness 0.7mm), axial fat-saturated T2-weighted TSE sequence with SPAIR (spectral adiabatic inversion recovery) (TR/TE 6150.0/83.0, FA 140, NEX 2, FOV 80x65mm, matrix 256x177, slice thickness 0.7mm), coronal T2-weighted HASTE (half-Fourier acquisition single-shot turbo spin-echo) sequence (TR/TE 577.0/172.0, FA 140, NEX 4, FOV 64x80mm, matrix 128x71, slice thickness 1mm), axial T1-weighted gradient-echo (GRE) sequence with volumetric interpolated breath-hold examination (VIBE) (TR/TE 10.0/5.1, FA 25, NEX 1, FOV 100x50mm, slice thickness 0.7mm) were acquired before administration of contrast media. Multiple axial enhanced T1-weighted GRE sequences with VIBE were obtained serially after contrast media injection to observe enhancement pattern.

4) Histopathologic analysis

All hamsters were serially sacrificed from 4th week to 12th week after acquisition of MRI (Fig 2). Midline incision was performed and the whole liver was extracted. After gross examination, the specimens were fixed in neutral buffered formalin (buffered 10% formaldehyde, pH 7.2) for histopathological processing. 4μm-thickness paraffin section of each lobe of the liver was processed for routine hematoxylin and eosine (H&E) staining. Additional sections for the hepatic masses were performed based on the

information provided from USG findings. Histopathologic examination was done by one pathologist focusing on the presence of CCA and other bile duct changes such as periductal inflammation, periductal fibrosis, cholangiofibrosis, cholangiofibroma, and biliary epithelial hyperplasia or dysplasia.

		Base-line	0wk	2wk	4wk	6wk	8wk	10wk	12wk
Group I (Control)	**1-1**	U	X	U	U Mc S				
	1-2	U	X	U	U	U	U	U Mc S	
	1-3	U	X	U	U	U	U Mc S		
	1-4	U	X	U	U	U	U	U	U Mc S
	1-5	U	X	U	U	U	U	U	U S
Group II (CS)	**2-1**	U	X	U	U Mc S				
	2-2	U	X	U	U	U	U	U Mc S	
	2-3	U	X	U	U	U	U	U	U Mc S
	2-4	U	X	U	U	U	U Mc S		
	2-5	U	X	U	U	U	U	U	U S
Group III (NMDA)	**3-1**	U	X	U	U Mc S				
	3-2	U	X	U	U	U	U	U Mc S	
	3-3	U	X	U	U	U	U	U	U Mc S
	3-4	U	X	U	U	U	U Mc S		
	3-5	U	X	U	U	U	U	U	U S
Group IV (CS+NMDA)	**4-1**	U	X	U	U	U M	U Mc S		
	4-2	U	X	U	U	U	U M	U Mc S	
	4-3	U	X	U	U	U	U	U M	U Mc S
	4-4	U	X	U	U	U	U	U M	U Mc S
	4-5	U	X	U	U	U M	U Mc S		
	4-6	U	X	U M	U Mc S				
	4-7	U	X	U M	U Mc S				
	4-8	U	X	U	U	U	U	U M	U Mc S
	4-9	U	X	U	U	U	U	U M	U Mc S

Figure 1. Grouping and experimental design of this study. Alphabet character in each cell represents the procedure or examination performed at each time point.

X : start of CS infection and NMDA feeding

U: ultrasonography (USG)

Mc: magnetic resonance imaging (MRI) with contrast enhancement

M: MRI without contrast enhancement

S: sacrifice

Results

There was no loss of hamsters during 12 weeks of experiments.

1) Chronological changes and representative findings of image and histopathologic findings

A) USG findings

On USG, all hamsters of Control group showed homogeneous low echogenicity of the liver similar to that of the human liver. There was no evidence of intrahepatic ductal dilatation or focal lesion in the liver (**Fig. 2**). There were small lymph nodes (LN) with the longest diameter less than 5mm. Some hamsters showed small amount of sediment in the gallbladder (**Fig. 3**). This finding was also noted in the hamsters of other groups in earlier weeks, even on the baseline USG. Thus, this finding was not counted as an abnormal finding and not included in the analysis of the results.

Two hamsters of NMDA group showed mildly increased periductal echogenicity (**Fig. 4**) and one hamster of NMDA group showed a LN with the longest diameter more than 5mm. Otherwise, USG finding in the hamsters of NMDA group was generally normal. There was no evidence of intrahepatic ductal dilatation or focal lesion in the liver. There was no significant abnormal finding in the gallbladder except some sediment.

The hamsters of CS group showed diffuse periductal echogenicity in the liver, intrahepatic ductal dilatation, LN enlargement with the longest

diameter more than 5mm, and sludge in the gallbladder (**Fig. 5**), but there was no mass in the liver. Some hamsters of CS group showed linear fluctuating structures in the gallbladder indicating live flukes (**Fig. 6**).

In addition to the findings noted in CS group, the hamsters of CS+NMDA group showed multiple hepatic masses and cysts. Hepatic masses showed increased echogenicity with hypoechoic rim on USG, which is similar to the finding of the human CCAs. (**Fig. 7**). Hepatic cysts appeared as small anechoic nodular lesion. USG findings are summarized in **Figure 8**.

(A)

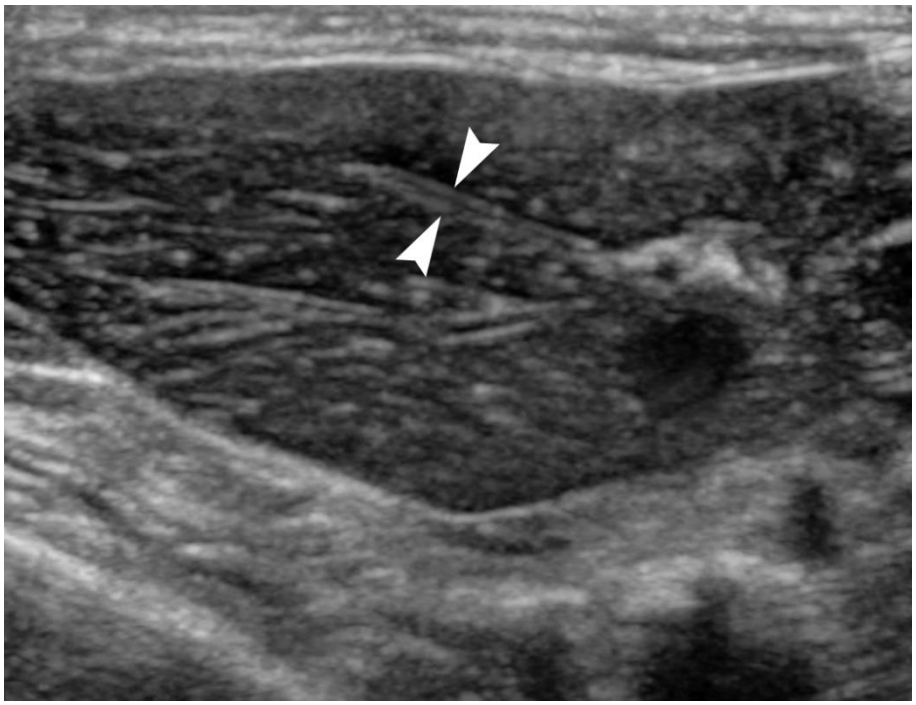

(B)

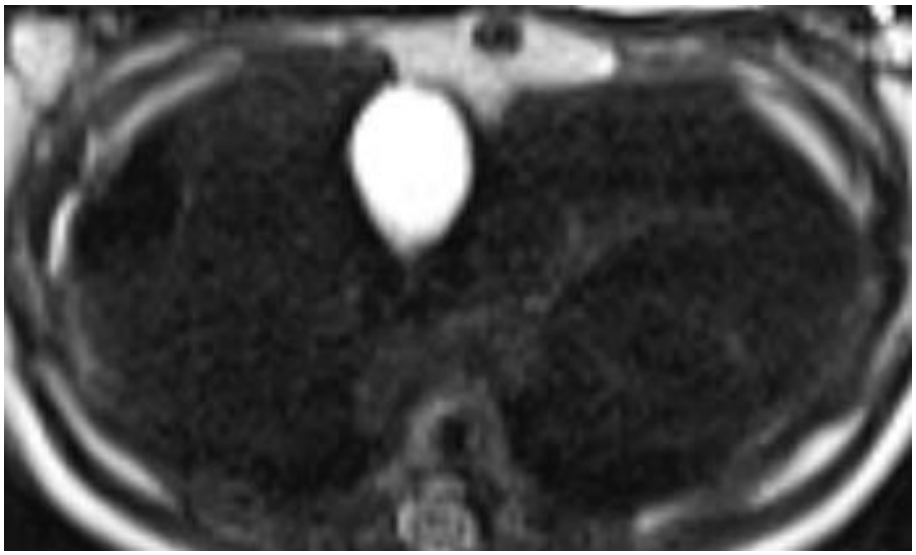

(C)

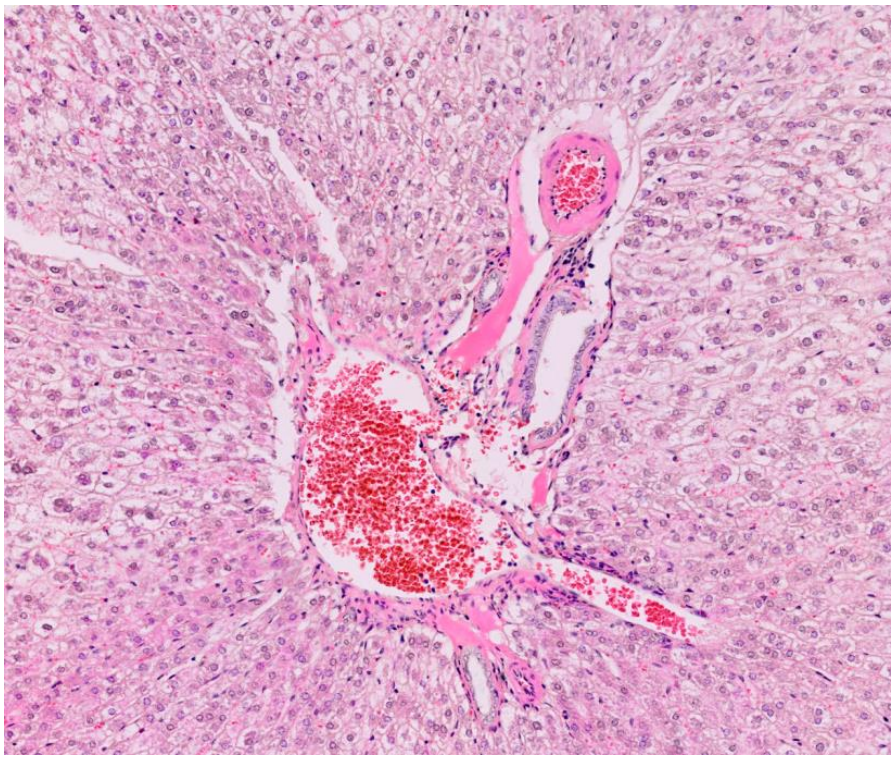

Figure 2. Representative USG, MRI and histopathologic finding of Control group. (A) USG was performed on a hamster in Control group at 10th week. USG shows homogeneous low echogenicity of right lobe of the liver similar to that of the human liver. Intrahepatic bile ducts were not distinguishable with the adjacent portal veins noted as thin echogenic lines (arrowheads). (B) Axial T2WI MRI shows homogeneous low signal intensity of the liver without significant focal lesion. Intrahepatic bile ducts were not dilated. There was no filling defect in the gallbladder. (C) On histopathologic examination, the liver showed normal appearance of bile ducts without evidence of inflammation or fibrosis. (H&E)

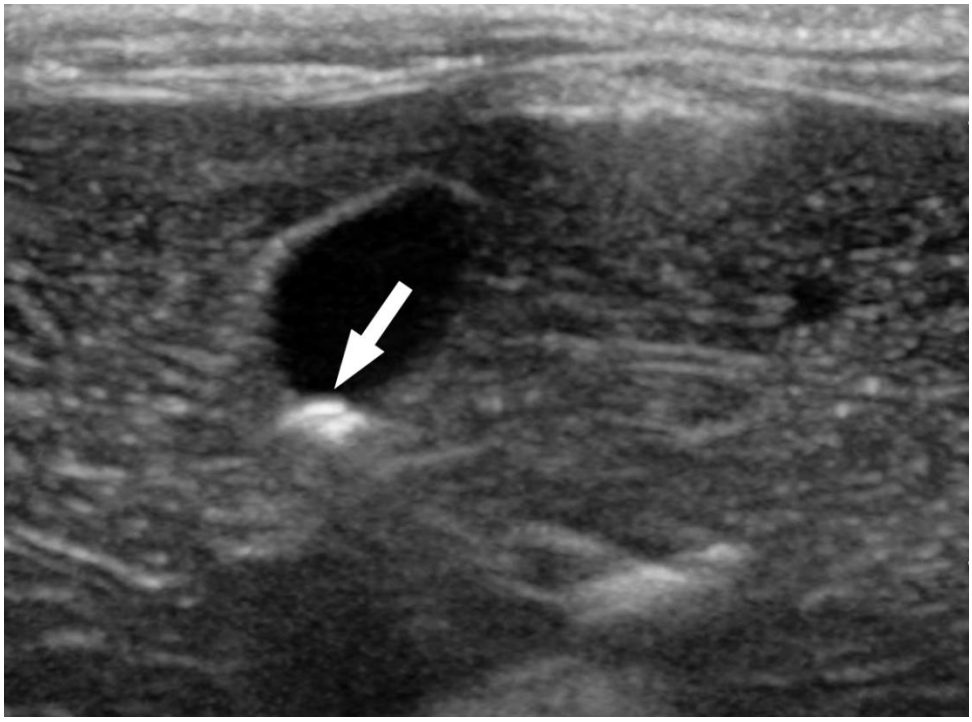

Figure 3. Sediments in the gallbladder. USG was performed on a hamster in Control group at 2nd week. Small echogenic lesion is noted in the dependent portion of the gallbladder (arrow). This finding was also noted in earlier weeks of the hamsters in other groups, which suggests that this is not an abnormal finding.

(A)

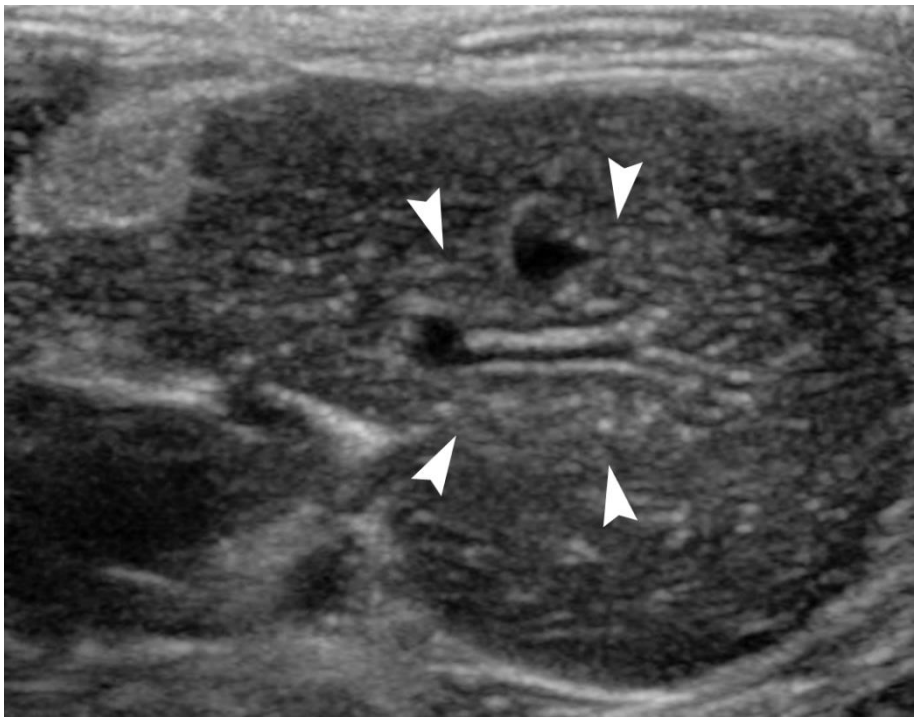

(B)

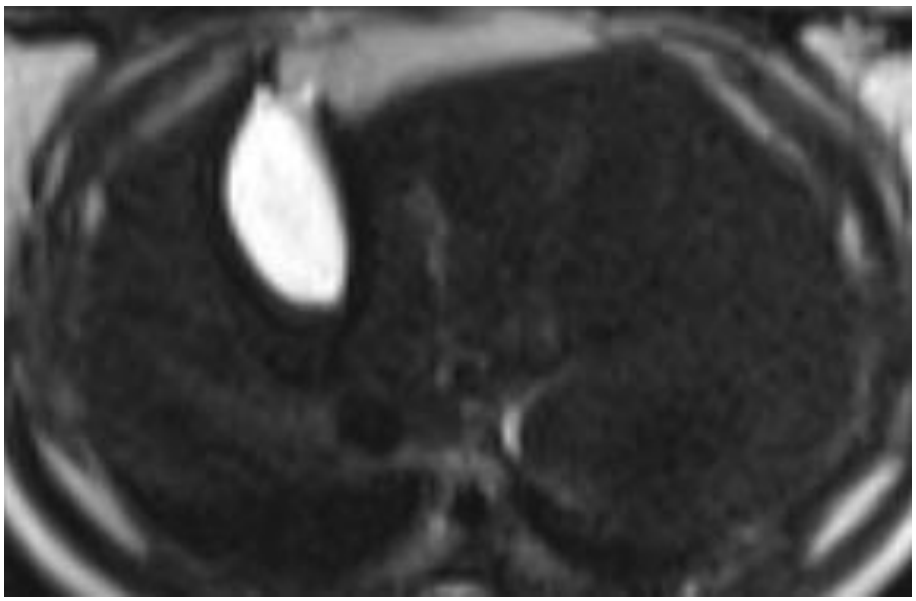

(C)

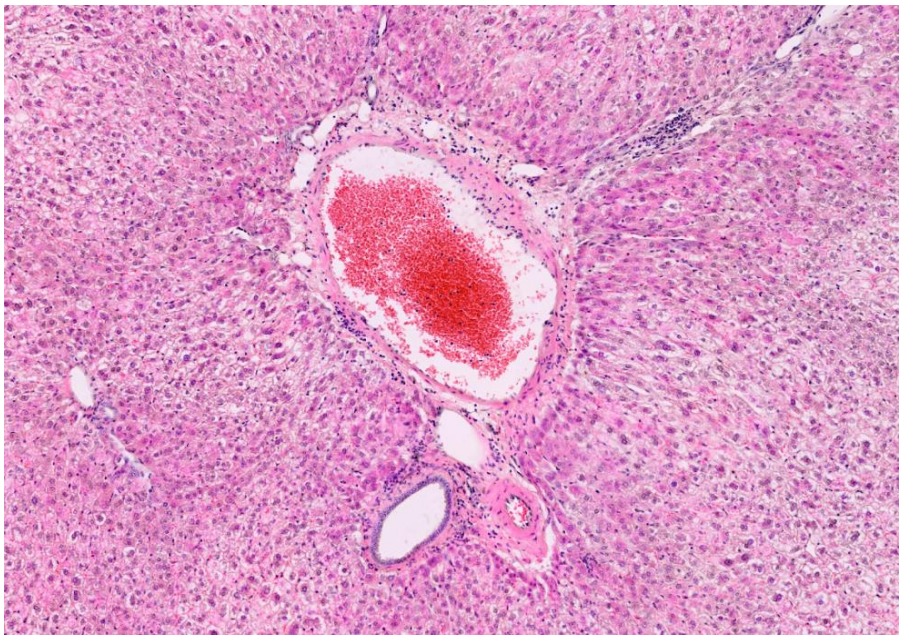

Figure 4. Representative USG, MRI and histopathologic findings of the livers in NMDA group. (A) USG was performed on a hamster in NMDA group at 4th week. Mild increased echogenicity is noted around portal vein (arrowheads). There is no evidence of intrahepatic ductal dilatation. (B) Axial T2WI MRI shows homogeneous low signal intensity of the liver without significant focal lesion or periductal signal change. Intrahepatic bile ducts were not dilated. There was no filling defect in the gallbladder. (C) On histopathologic examination, the liver showed normal appearance of bile ducts without evidence of inflammation or fibrosis. (H&E)

(A)

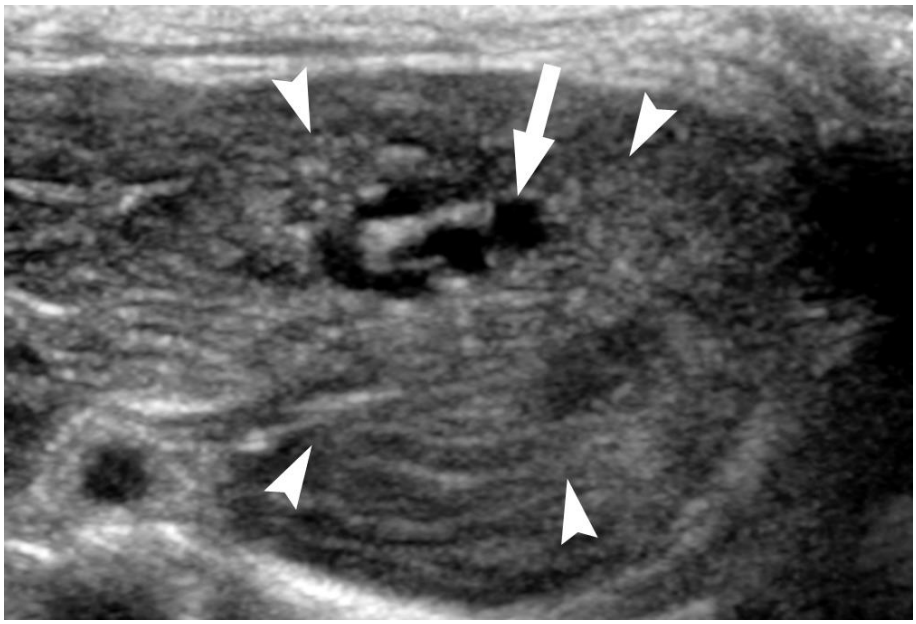

(B)

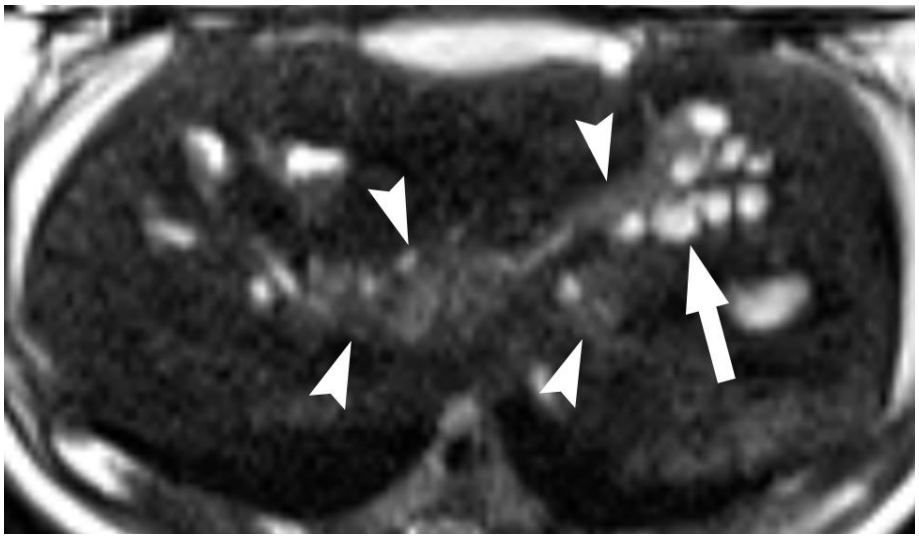

(C)

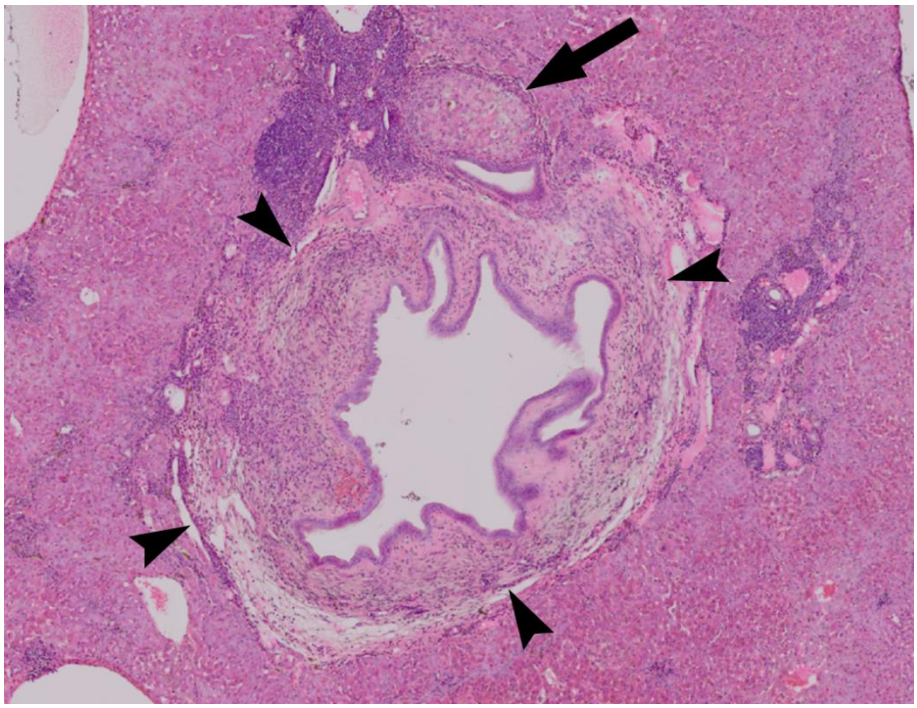

Figure 5. Representative USG, MRI and histopathologic findings of the livers in CS group. (A) USG was performed on a hamster in NMDA group at 12th week. Diffuse increased echogenicity (arrowheads) is noted around irregularly dilated intrahepatic bile ducts (arrow). There is no evidence of mass in the liver. (B) Axial T2WI also shows high signal intensity (arrowheads) around tortuously dilated intrahepatic bile ducts (arrow). (C) On histopathologic examination, the liver showed biliary epithelial hyperplasia, periductal fibrosis (black arrowheads), inflammatory cell infiltration, and egg granuloma (black arrow). (H&E)

(A)

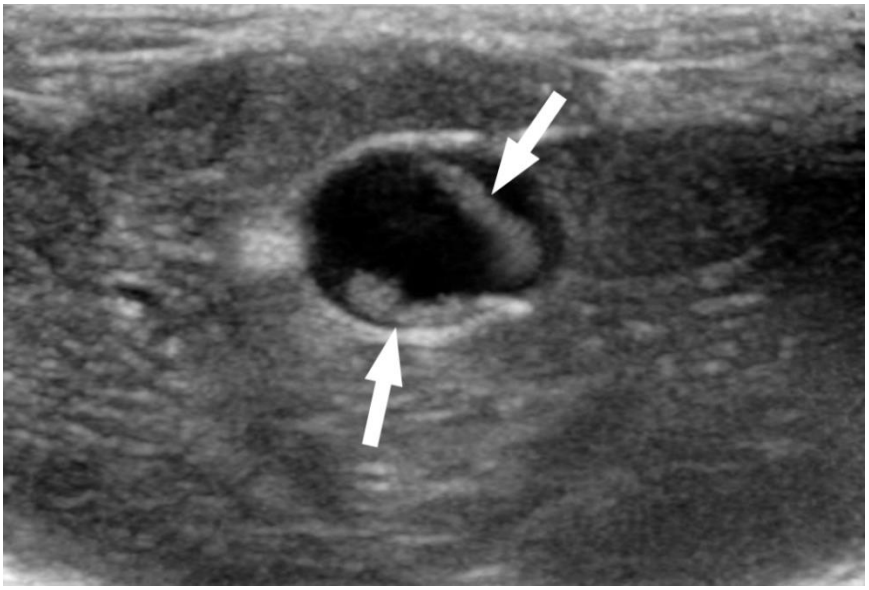

(B)

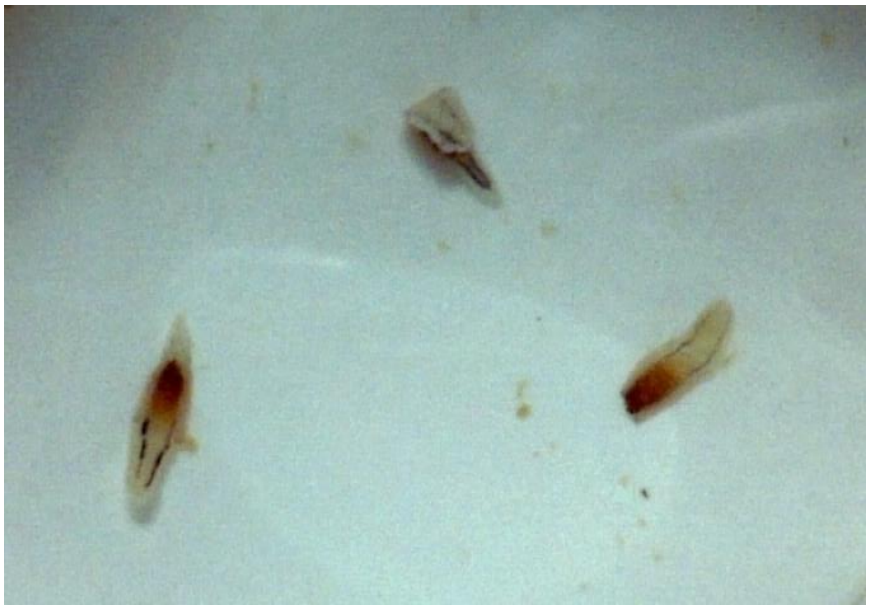

Figure 6. Live flukes in the gallbladder. USG was performed on a hamster in CS group at 4th week. (A) Linear fluctuating structures were noted in the gallbladder indicating live flukes in the gallbladder (arrows). (B) On gross examination, multiple liver flukes came out of the gallbladder after incision.

(A)

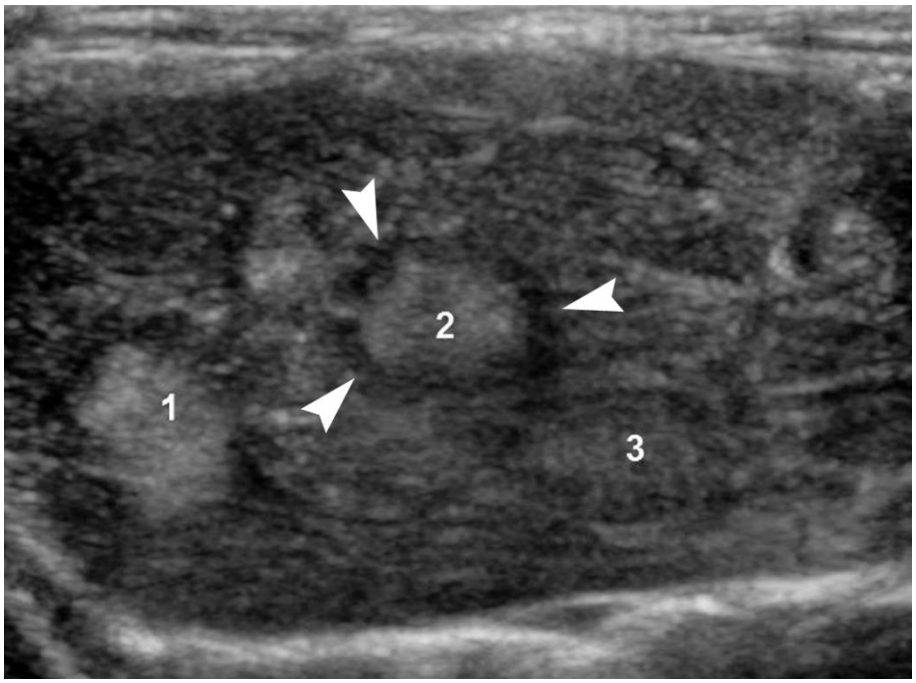

(B)

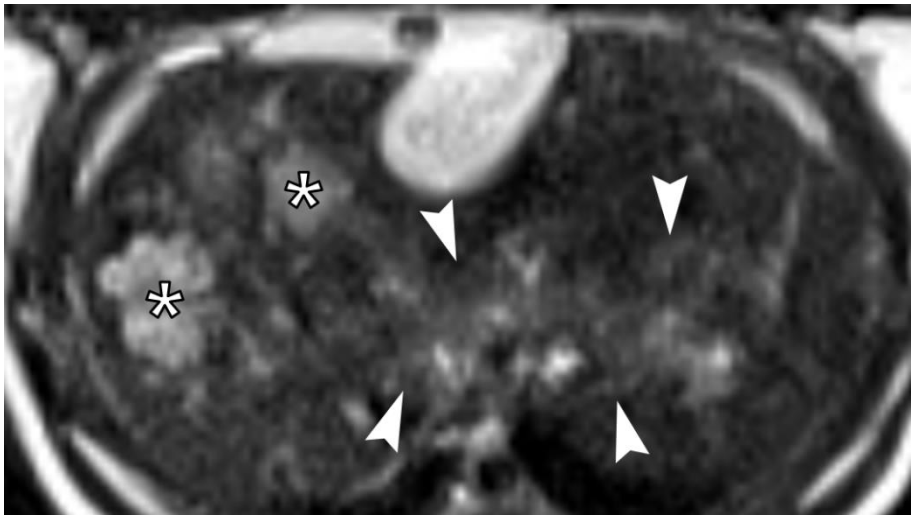

(C)

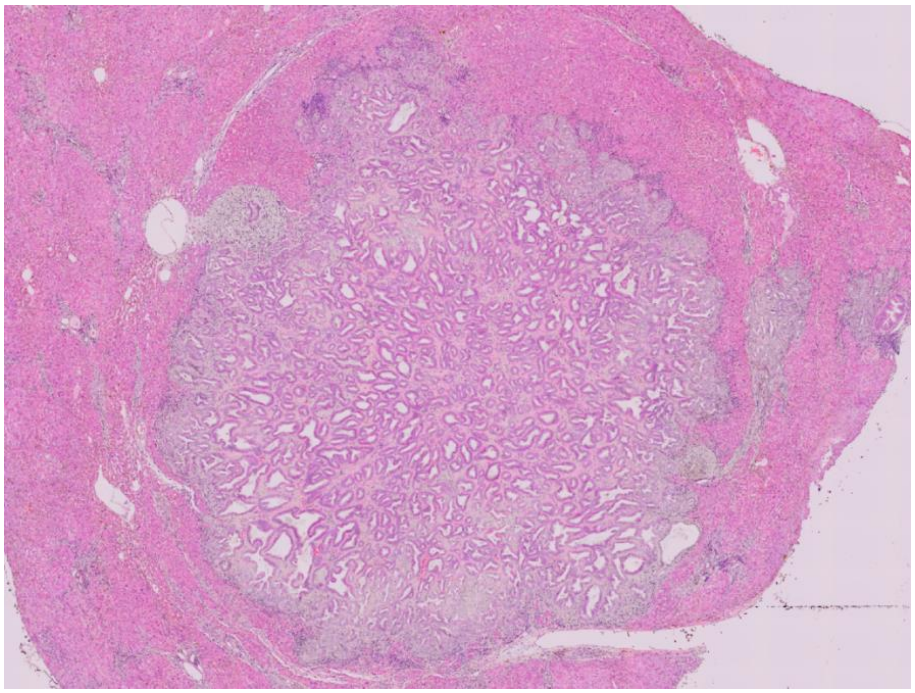

Figure 7. Representative USG, MRI and histopathologic findings of the livers in CS+NMDA group. (A) USG was performed on a hamster in NMDA group at 10th week. Multiple masses were noted in the right lobe of the liver (numbers). The masses show increased echogenicity with hypoechoic rim (arrowheads). (B) Axial T2WI MRI also shows multiple masses with high signal intensity with hypointense rim (asterisks). Diffuse high signal intensity around intrahepatic bile ducts was also noted (arrowheads). (C) The masses were confirmed as cholangiocarcinoma on histopathologic examination, which was characterized by proliferative cholangioles lined by pleomorphic cells, architectural distortion, and fibrous stroma. (H&E)

	Group I (Control)							Group II (CS)							Group III (NMDA)							Group IV (CS+NMDA)						
Findings	e	E	d	n	s	c	m	e	E	d	n	s	c	m	e	E	d	n	s	c	m	e	E	d	n	s	c	m
2 wk								5			3							1				7	2		4	2		
4 wk									5	3	1	1			2								7	4	5			
6 wk										2		2			1									2		2	1	2
8 wk																								1		1		2
10 wk												1																2
12 wk																												

Figure 8. Summarized results of USG findings. The number in each cell represents the number of hamsters in which the corresponding finding was firstly detected at each time point. In CS and CS+NMDA groups, periductal echogenicity and lymph node enlargement appeared in the earlier weeks, followed by intrahepatic ductal dilatation. Hepatic masses and large cyst in the liver appeared after 6th week of infection in CS+NMDA group.

e: mild periductal echogenicity

E: diffuse periductal echogenicity

d: intrahepatic ductal dilatation

n: LN node of long diameter more than 5mm

s: sludge in the gallbladder

c: large cyst

m: mass

B) MRI findings

Overall, MRI finding were well correlated with USG findings. The periductal echogenicity noted on USG appeared as periductal high signal intensity in contrast to the background low signal intensity of liver parenchyma on T2WI. Dilated intrahepatic ducts appeared as tubular cystic structure of bright signal intensity on T2WI. Sludge in the gallbladder appeared as a filling defect. Hepatic masses showed high signal intensity with hypointense rim on T2WI and low signal intensity on T1WI. According to our study, axial T2-weighted TSE sequence with navigator-triggered PACE was the most useful sequence to evaluate abnormalities in the liver. This sequence showed good signal-to-noise ratio and sub-millimeter spatial resolution with minimal motion artifact. Overall, T2WI visualized chronological changes of the liver in CS+NMDA groups (**Table 1**).

Due to the lack of accessible peripheral venous route and rapid circulation in the hamsters, it was not sufficiently feasible to acquire dynamic enhanced MRI although we took enhanced MRI as soon as we injected contrast media into the left ventricle. In Control and NMDA groups, the time of contrast media excretion into the gallbladder was measured as 7.6 (3-16) minutes on average. On the other hand, it was delayed as 52.9 (6-136) minutes in CS and CS+NMDA groups. Due to the delayed biliary excretion of contrast media in CS and CS+NMDA groups, analysis of enhancement pattern of the hepatic masses on the hepatobiliary phase was limited. Moreover, as we used free-breathing VIBE sequence for faster acquisition, enhanced MRI images

were contaminated with motion artifact.

2nd week	4th week	6th week	8th week	10th week	12th week
mild periductal high SI	periductal high SI irregular BDD small cyst	periductal high SI irregular BDD small cyst mass	periductal high SI irregular BDD small cyst mass	periductal high SI irregular BDD small cyst large cyst mass	periductal high SI irregular BDD small cyst large cyst mass

Table 1. Summarized results of MRI findings detected in the hamsters of CS+NMDA group. Overall, MRI findings detected on T2WI were well correlated with USG findings.

SI: signal intensity

BDD: bile duct dilatation

C) Histopathologic findings

On histopathologic examination, the livers of Control group showed normal appearance of hepatocytes, cholangiocytes and portal triad without evidence of inflammation. The histopathologic findings of the livers of NMDA group were also normal similarly to those of Control group. CS group showed inflammatory cell infiltration, biliary epithelial hyperplasia, and periductal fibrosis. Dilated bile ducts containing worms and egg granulomas were also noted. There was no cholangiocarinoma in CS group.

CS+NMDA group also showed the inflammatory findings noted in CS group including biliary epithelial hyperplasia, periductal fibrosis, worms within the dilated bile ducts, and egg granulomas. Moreover, CS+NMDA group showed cystic ductal atypical hyperplasia, ductal dysplasia, cholangiofibrosis and cholangiocarcinoma. Cholangiocarcinomas in the hamsters of CS+NMDA group was characterized by proliferative cholangioles lined by pleomorphic cells, architectural distortion, and fibrous stroma (**Fig. 7C**).

2) Lesion-to-lesion comparison of image and histopathologic findings

A) Ductal dilatation

Both CS and CS+NMDA group showed intrahepatic ductal dilatation and periductal echogenicity, but their dilatation patterns were slightly different.

In CS group, MRI shows tortuously and irregularly dilated intrahepatic ducts with surrounding periductal echogenicity or increased signal intensity. In CS+NMDA group, intrahepatic ducts were also irregularly dilated, but they seemed to be interrupted by periductal echogenicity or increased signal intensity. On USG, ductal dilatation seemed to be less prominent on CS+NMDA group than on CS group, which was well correlated with MRI finding. On enhanced MRI, dilated bile ducts were visualized as nonenhancing tubular structures. In CS group, histopathologic examination revealed dilated intrahepatic ducts surrounded by thick periductal fibrosis. On the other hand, intrahepatic ducts in CS+NMDA group showed were narrowed by periductal fibrosis. (**Fig. 9**)

(A)

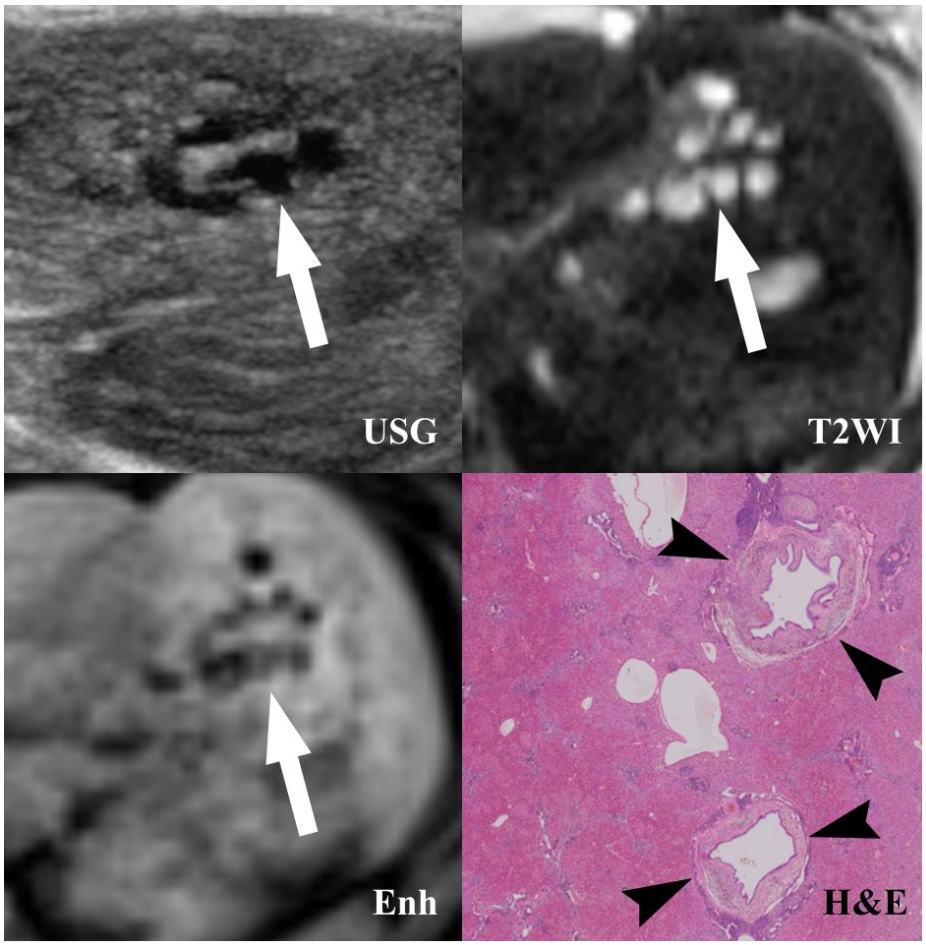

(B)

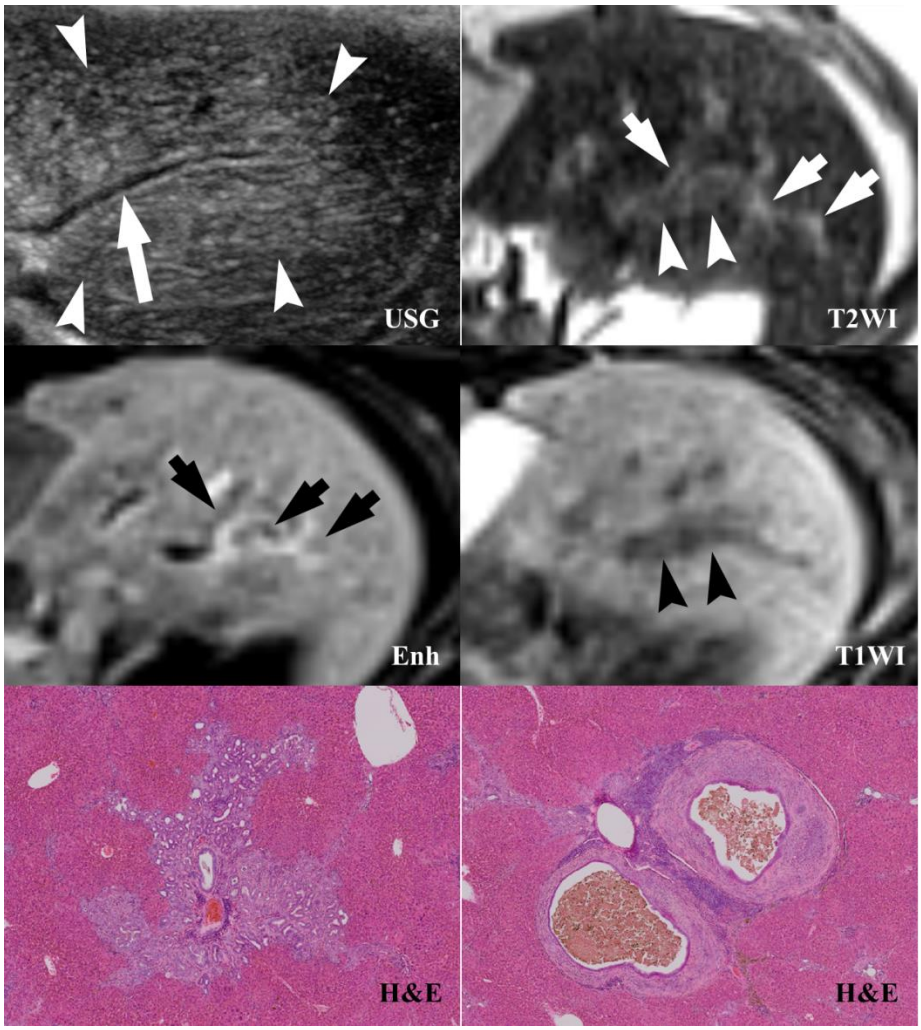

Figure 9. Different patterns of ductal dilatation between CS and CS+NMDA groups. (A) USG, MRI, and histopathologic findings of bile duct dilatation in CS group. USG and T2WI MRI showed tortuously dilated intrahepatic bile ducts, which were visualized as nonenhancing tubular structures on enhanced MRI (white arrows). Note the signal intensity of dilated intrahepatic bile ducts on T2WI is much brighter than surrounding periductal increased signal intensity, which is compatible to the finding of cystic structures.

Histopathologic examination revealed dilated intrahepatic ducts surrounded by periductal fibrosis (black arrowheads).

(B) USG, MRI, and histopathologic findings of bile duct dilatation in CS+NMDA group. USG showed diffuse increased echogenicity (white arrowheads) along the left portal vein (long white arrow). Bile duct dilatation was not prominent. T2WI MRI also showed periductal high signal intensities (white arrowheads) without dilated intrahepatic bile ducts. Note the signal intensity of intrahepatic bile ducts (show white arrows) is slightly brighter than surrounding periductal increased signal intensity, which is unusual finding to simple cystic structures. On enhanced MRI, intrahepatic ducts were visualized as poorly enhancing tubular structures (short black arrows). Note the size of poorly enhancing tubular structure is different to the size of periductal increased signal intensity on T2WI. This finding suggests that periductal increased signal intensity on T2WI in CS+NMDA group does not contain only periductal fibrosis or inflammatory cell infiltration, but also ductal or intraductal pathology. On T1WI, periductal lesions show decreased signal intensity (black arrowheads). Histopathologic examination of the left hepatic lobe revealed dysplastic change (left lower image) and hemorrhage within the intrahepatic bile ducts and periductal fibrosis (right lower image). Thus, the discrepancy of the periductal lesion between T2WI and enhanced MRI might be contributed by dysplastic change or intraductal hemorrhage.

B) Hepatic cysts

Many cysts were detected in the livers of CS+NMDA group on both USG and MRI, whereas there was no cyst in the livers of other three groups. Most of them were small cysts usually less than 3mm, but one cyst was larger than 5mm. The large cyst was detected on USG as early as 6^{th} week presenting with its size of 7.4mm and progressively enlarged to 9.6mm until 12^{th} week. The cyst was a unilocular cyst with internal linear structure, which can be a dead worm, septum, or debris. On histopathologic examination, the cyst was a true epithelial cyst lined by biliary epithelial cells with metaplasia. There were fibrosis, inflammatory cell infiltration, and egg granulomas around the cyst. Considering the fact that the cyst was lined by biliary epithelial cells, the cyst was thought to be formed by ballooning of bile ducts, not by pseudocyst or abscess formation (**Fig.10**).

Other small cysts were usually less than 3mm. Some of the small cysts detected on USG were later determined to be focally dilated ducts because direct connectivity between the cyst and adjacent dilated intrahepatic ducts were noted on follow-up MRI. Some of the small cysts showed pooling of contrast media on 25min-delayed hepatobiliary phase enhanced MRI, which suggests that the cysts have communication with the biliary system. Considering that interrupted pattern of ductal dilation in CS+NMDA group and pooling of contrast media in the cysts, many of the small cysts detected on USG or MRI might be actually focally dilated intrahepatic ducts (**Fig. 11**).

(A)

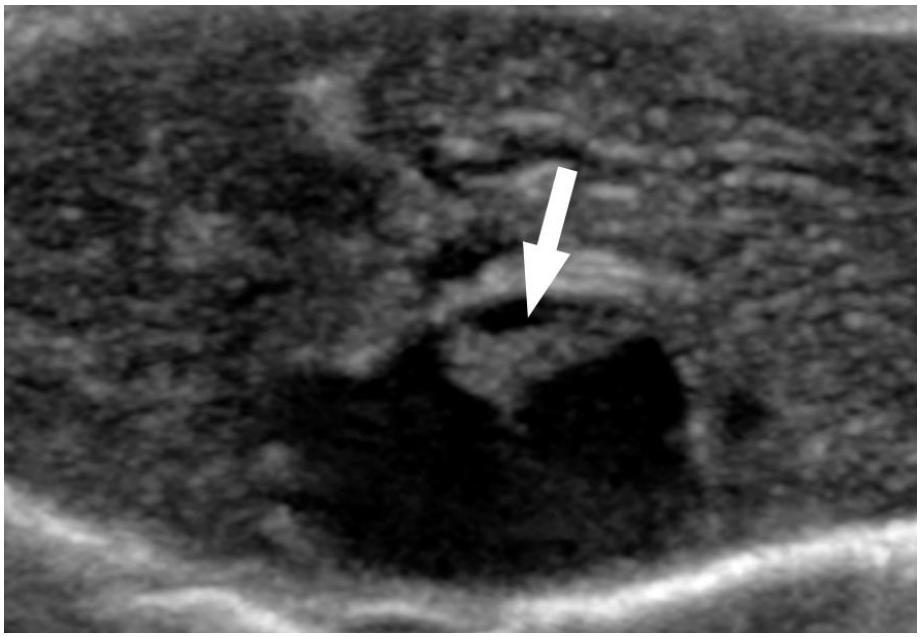

(B)

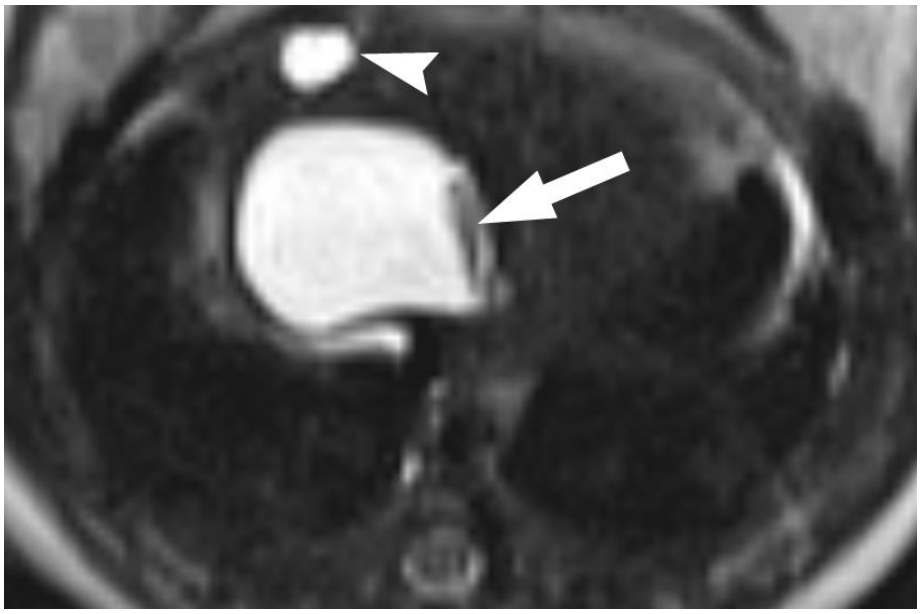

(C)

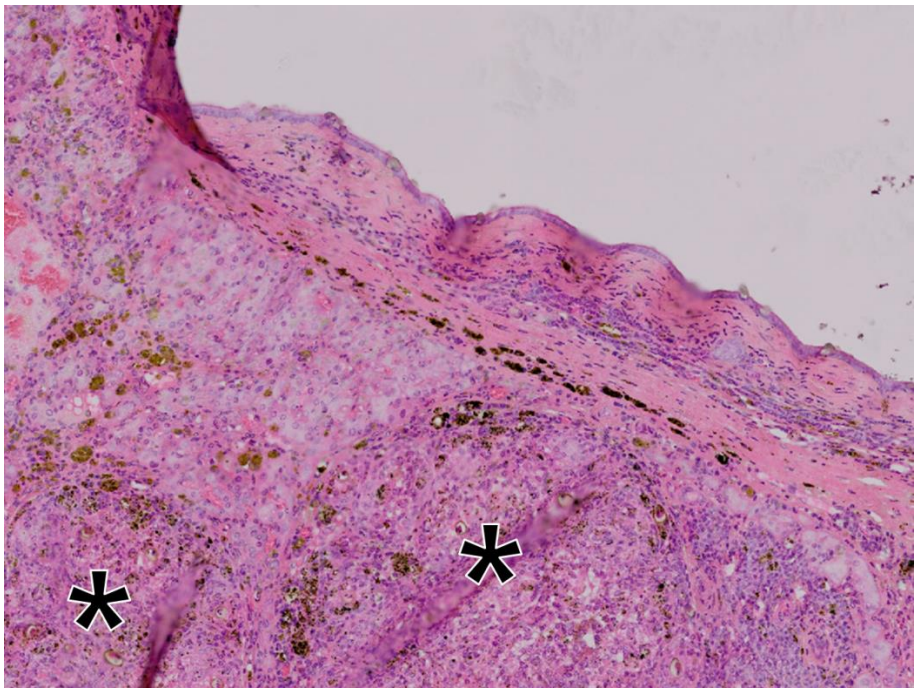

Figure 10. A large cyst in CS+NMDA group. USG was performed on a haster in CS group at 6th week. (A) Unilocular cystic lesion with internal non-moving linear structure (arrow) was detected in the middle hepatic lobe. (B) On MRI, there was no evidence of mural nodule or thickened wall except the internal linear structure (arrow). Note the dilated intrahepatic duct (arrowhead). (C) On histopathologic examination, the cyst was a true epithelial cyst lined by biliary epithelial cells surrounded by fibrosis and egg granulomas (black asterisks). (H&E)

(A)

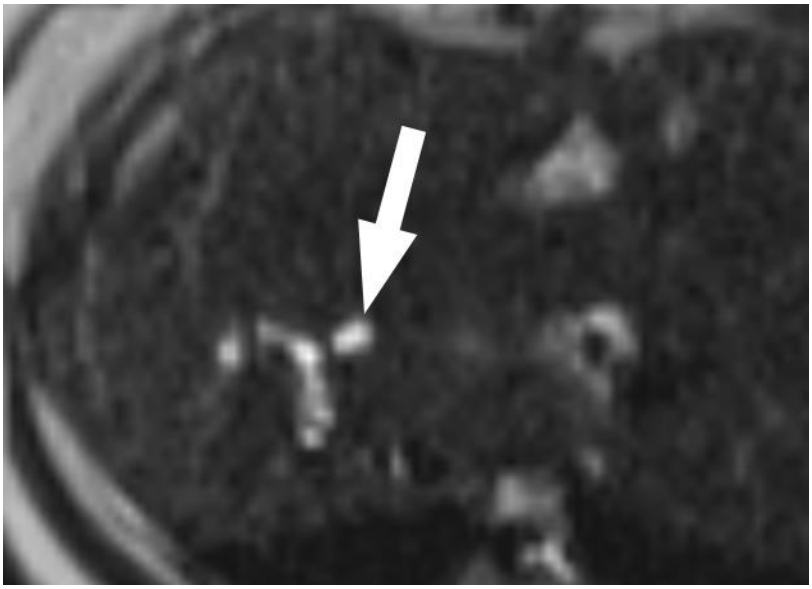

(B)

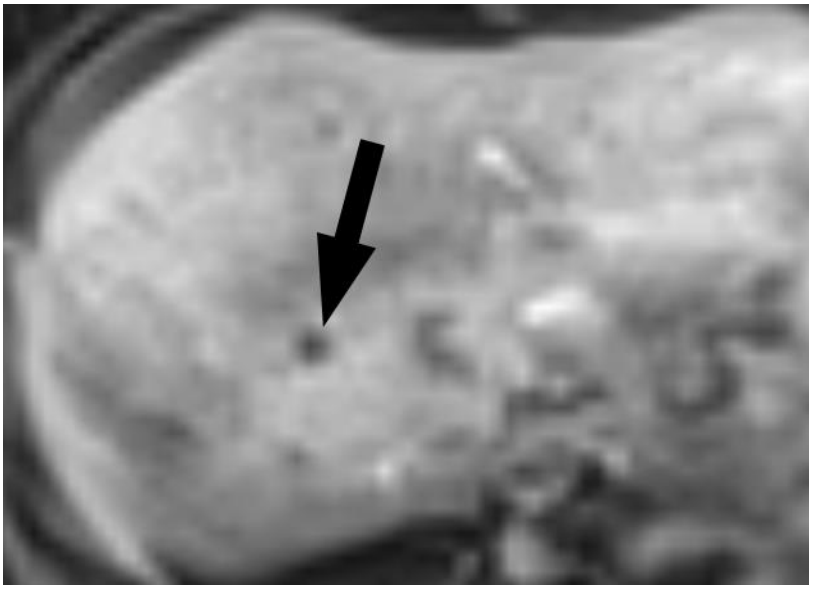

(C) 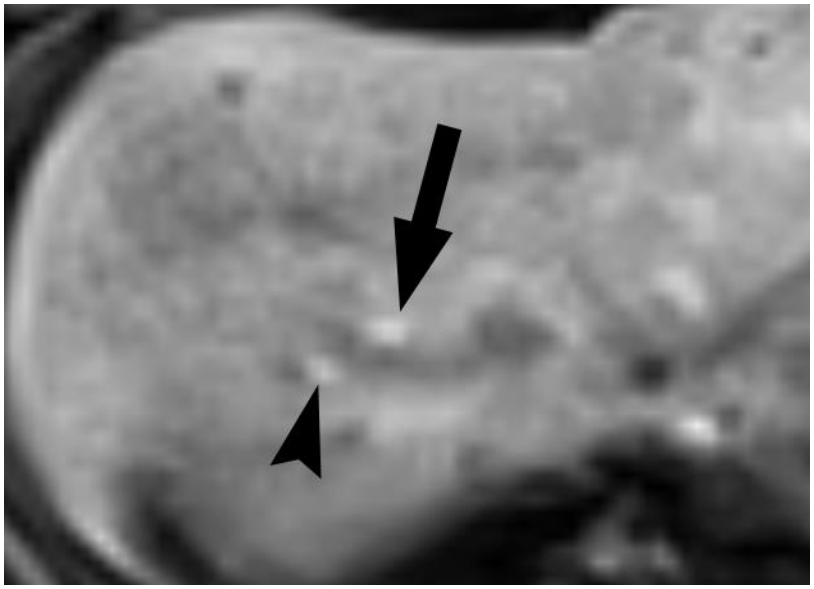

Figure 11. Small cysts in CS+NMDA group. (A) T2WI shows a small cystic lesion of bright signal intensity in the middle hepatic lobe (arrow). (B) On enhanced MRI of early phase, the cystic lesion does not enhance (arrow). (C) On enhanced MRI of hepatobiliarya phase, the cystic lesion shows higher signal intensity than surrounding liver parenchyma, probably due to pooling of contrast media (arrow). This finding suggests that the cystic lesion has communication with biliary system. Note similar high signal intensity of adjacent intrahepatic bile duct (arrowhead).

C) Hepatic masses

The hamsters of CS+NMDA group showed multiple hepatic masses. On the other hand, there was no mass in the liver in other groups (Control, CS, and NMDA) during 12 weeks of follow-up period. The first hepatic mass was noted as early as 6th week and every living hamster in CS+NMDA group at 10th week had at least one hepatic mass per each hamster. USG detected 15 hepatic masses in 6 hamsters of CS+NMDA group. MRI also detected 15 hepatic masses, although not all hepatic masses detected by MRI were same as those detected by USG (**Fig. 12**).

MRI detected two additional lesions to USG. Both lesions were located in the superior portion of the middle lobe of the liver, which suggests that USG has some limitation to detect focal lesions highly located in the liver probably due to limited sonic window by the diaphragm and rib cage. One lesion was CCA and the other lesion was not identified on histopathologic examination. USG also detected two additional lesions to MRI. Both lesions were located in the left lobe of the liver and identified later by a retrospective review of MRI. One lesion was determined as a pseudolesion due to partial volume artifact of periductal echogenicity by a review of MRI. The other lesion was determined as biliary dysplasia on histopathologic examination. For the 13 hepatic masses detected by both USG and MRI, 9 lesions were CCAs, one lesion was cholangiofibroma, and the other 3 lesions were not identified on histopathologic examination.

On histopathologic examination of the livers of CS+NMDA group,

14 hepatic masses were identified, which includes 12 CCAs. Among them, USG and MRI were able to demonstrate 9 and 10 CCAs respectively. The two CCAs that both USG and MRI could not detect were located in the right lobe of the liver and their sizes were 2.4mm and 2.2mm. The two CCAs were identified later by a retrospective review of MRI, although there is no solid evidence of exact matching.

There were two precancerous lesions in 14 pathologically confirmed hepatic masses. One of them was biliary dysplasia and the other was cholangiofibroma (**Fig. 13**). Both lesions showed high signal intensity on T2WI and low signal intensity on enhanced MRI. There was no significant difference of image finding between CCAs and these precancerous lesions. MRI findings of hepatic masses are summarized in **Table 2**.

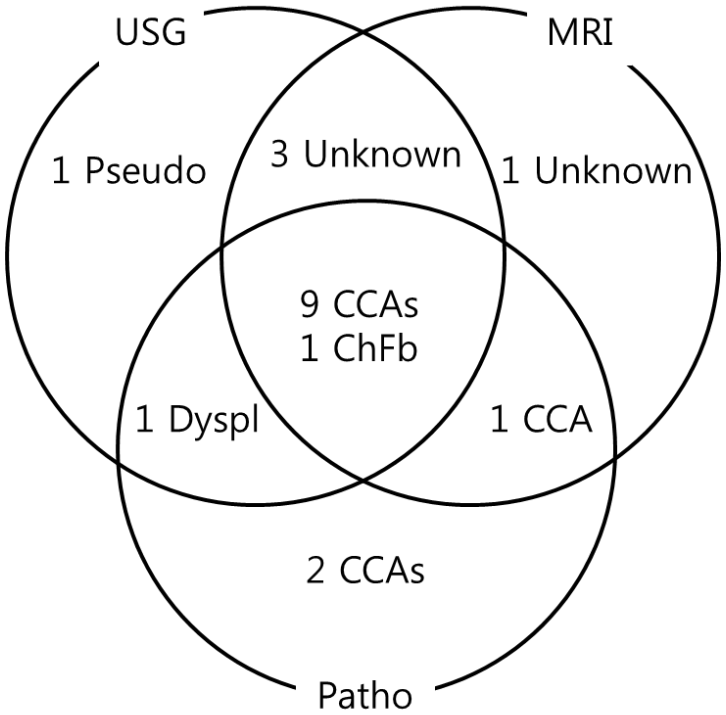

CCA: cholangiocarcinoma

ChFb: cholangiofibroma

Dyspl: dysplasia

Pseudo: Pseudolesion

Figure 12. Results of hepatic masses in CS+NMDA group detected by USG, MRI, and histopathologic examination. USG and MRI independently detected 15 hepatic masses, which includes 10 CCAs, one dysplasia, and one cholangiofibroma. Histopathologic examination detected 12 CCAs in total. The two CCAs only detected by histopathologic examination and one dysplasia detected by USG were identified later by a retrospective review of MRI, although there is no solid evidence of exact matching.

(A)

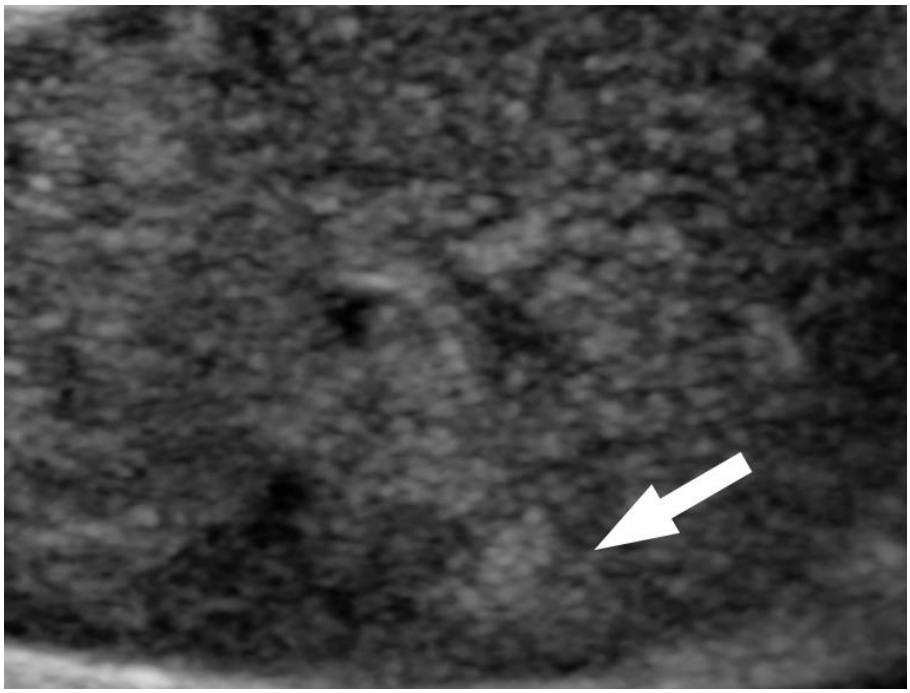

(B)

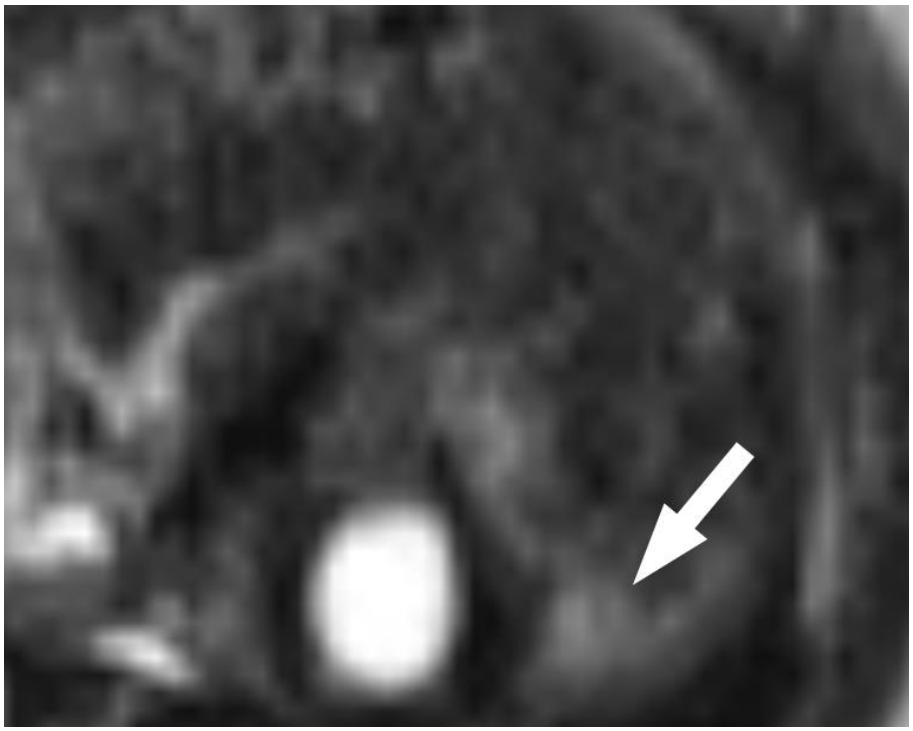

(C)

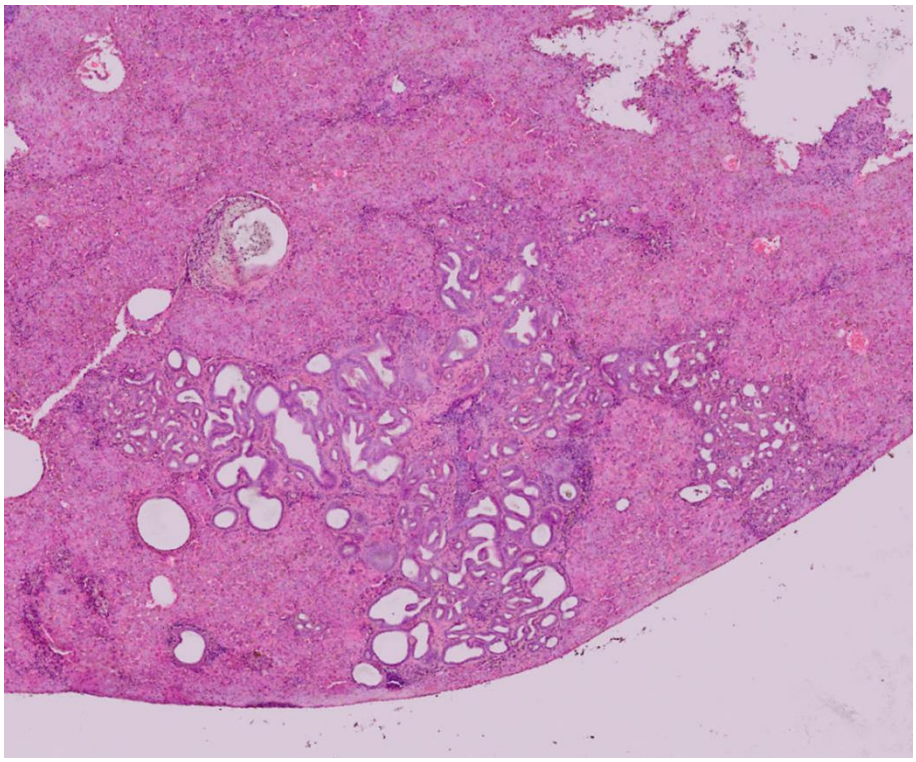

(D)

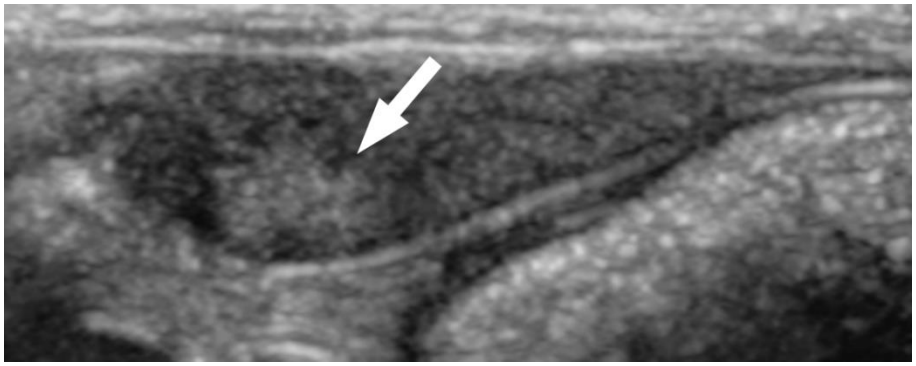

(E)

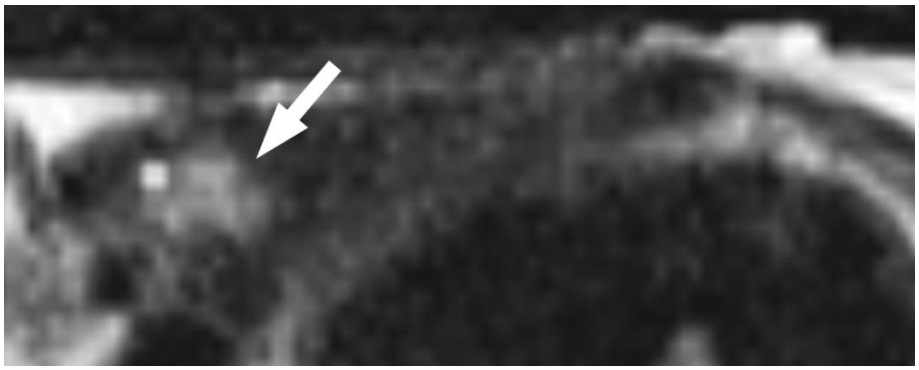

(F)

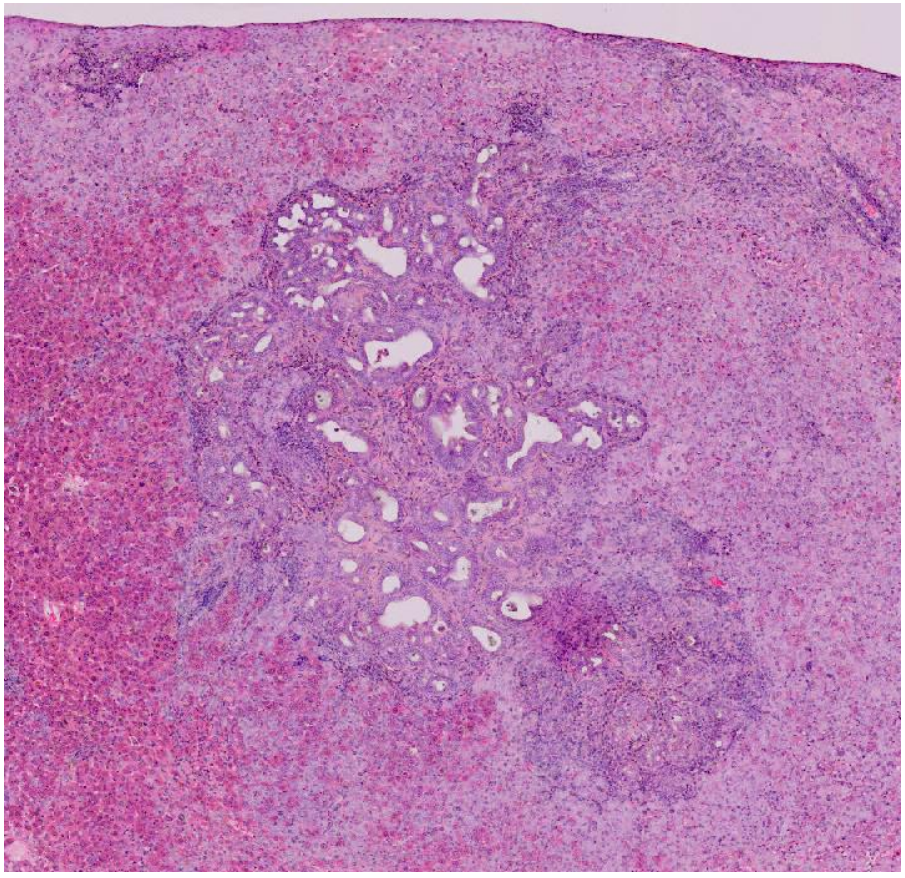

Figure 13. USG, MRI and histopathologic findings of precancerous lesions in CS+NMDA group. (A) On USG performed at 12th week, echogenic nodular lesion with subtle hypoechoic rim was suspected in the superior portion of the left hepatic lobe (arrow). (B) Axial T2WI shows ill-defined lesion with increased signal intensity in the left hepatic lobe (arrow). (C) On histopathologic examination, the lesion was confirmed as ductal dysplasia. (D) On USG performed at 10th week, echogenic nodular lesion with hypoechoic rim was noted in the inferior portion of the left hepatic lobe (arrow). (E) On T2WI, the nodular lesion showed high signal intensity with suspicious hypointense rim (arrow). These image findings are similar to those of CCAs. (F) Histopathologic examination revealed that the lesion was cholangiofibroma.

Hamster	Week	Diagnosis	Detection		Location	Size (mm)	T2WI	T1WI	HB phase
			USG	MRI[1)]					
4-1	8	CCA	O	O	Left	6.3	High	Low	High
4-1	8	Unidentified	X	O	Middle	3.1	High	Low	High
4-2	10	Unidentified	O	O	Middle	3.3	High	Low	Low
4-2	10	Cholangiofibroma	O	O	Left	3.8	High	Low	Low
4-3	12	Pseudolesion[2)]	O	X	Left	4.4	High	Low	High
4-3	12	CCA	X	X	Right	2.7	High	Low	High
4-3	12	CCA	O	O	Middle	11.9	High	Low	Low
4-3	12	CCA	O	O	Right	6.7	High	Low	Low
4-4	12	Unidentified	O	O	Left	3.8	High	Low	Low
4-4	12	CCA	X	X	Right	2.8	High	Low	Low
4-8	12	CCA	O	O	Middle	8.3	High	Low	High
4-8	12	CCA	O	O	Middle	3.8	High	Low	High
4-8	12	Unidentified	O	O	Left	3.3	High	Low	Low
4-9	12	CCA	O	O	Middle	5.9	High	Low	Low
4-9	12	CCA	X	O	Middle	5.7	High	Low	Limited[3)]
4-9	12	CCA	O	O	Middle	5.6	High	Low	Low
4-9	12	CCA	O	O	Middle	6.6	High	Low	Low
4-9	12	CCA	O	O	Right	4.4	High	Low	Low
4-9	12	Dysplasia	O	X	Left	3.4	High	Low	Limited[3)]

[1] The recorded detectability of MRI was based on the initial assessment of MRI. All lesions were able to be located on retrospective review of MRI.

[2] This lesion was determined as a pseudolesion due to partial volume artifact of periductal echogenicity by a review of MRI.

[3] Evaluation of enhancement was limited due to motion artifact.

HP phase: hepatobiliary phase

Table 2. Summarized results of MRI findings of hepatic masses. All hepatic masses showed high signal intensity on T2WI and low signal intensity on T1WI despite of various histopathologic diagnosis. The enhancement degrees of hepatic masses on hepatobiliary phases were various, showing higher or lower signal intensity than liver parenchymal enhancement. Analysis of enhancement pattern of the hepatic masses on the hepatobiliary phase was limited due to the delayed biliary excretion of contrast media. The hepatobiliary phases were obtained at 25:33 after contrast media injection on average.

Discussion

In our study, CCAs appeared in the hamsters of CS+NMDA group as early as 6th week of infection. There were a total of 12 CCAs and 10 of them were demonstrated by USG or MRI. USG and MRI also showed other findings of disease progression such as periductal increased echogenicity or signal intensity, ductal dilatation, complicated cysts, and sludges in the gallbladder. These findings are well correlated with the results of previous reports [7, 10].

USG showed good performance on detecting CCAs, but it was not a suitable modality in monitoring of the precancerous lesions of CCA. On USG, periductal echogenicity was noted in the earlier weeks of CS and CS+NMDA groups, but after that, the periductal echogenicity expanded and covered the liver diffusely, which can potentially mask early precancerous lesions. Moreover, as USG is a subjective study mainly dependent to the operators' skills and does not cover whole section of the liver, retrospective analysis of the precancerous or cancerous lesions detected at later time point was limited.

To our best knowledge, this study is the first attempt of liver MRI to detect CCAs and precancerous lesions in the hamsters. Axial T2-weighted TSE sequence with navigator-triggered PACE was the most useful sequence of MRI. T2-weighted TSE clearly demonstrated various findings such as periductal signal change, ductal dilatation, and hepatic focal lesions including CCAs and complicated cysts. Navigator-triggered PACE technique minimized breath motion artifact and produced images of good signal-to-noise ratio and

sub-millimeter spatial resolution. This sequence was performed within tolerable time of about 7 to 10 minutes depending on the respiratory rate.

Although axial T2-weighted TSE sequence with navigator-triggered PACE was useful in evaluating abnormalities in the liver, both periductal inflammatory change and CCA showed high signal intensity on T2WI. This implies that the precancerous lesion as a middle stage from periductal inflammatory change to CCA would also show high signal intensity on T2WI. This is also supported by the results that the masses determined as biliary dysplasia and cholangiofibroma showed high signal intensity on T2WI. Thus, the precancerous lesions may not be differentiated with periductal inflammatory change or CCAs by the signal intensity only. To overcome this limitation, sequences such as diffusion-weighted image (DWI) or functional MRI, which can show more information than signal intensity, would be needed. More advanced enhancement MRI sequences such as parallel imaging with higher acceleration or radial gradient echo sequence [11, 12], which has better temporal resolution and robustness on motion artifact, might elucidate the enhancement pattern of precancerous lesions. As MR units of higher magnetic field strength are thought to provide images of better spatial and temporal resolution [13], further studies using MR units of higher magnetic field strength might be helpful to detect small or subtle precancerous lesions.

USG-guided left ventricular puncture can be an effective method to inject contrast media into hamsters. Since there was no sufficient tail vein to catheterize in hamsters, it is not so easy to inject contrast media intravenously. There are articles about sampling methods of hamsters using the saphenous or

jugular veins [14, 15], but we could not succeed in catheterizing and injecting sufficient amount of contrast media into those vessels under the guidance of USG. Then, we tried USG-guided left ventricular puncture and could deliver sufficient amount of contrast media into the intravascular space in bolus. We observed the hamsters about 24 hours after the left ventricular punctures for potential casualties, but there was no loss in all of 21 hamsters receiving left ventricular punctures, although there is a possibility of late complication such as cardiac tamponade or hemothorax.

There are some limitations in our study. First, histopathologic examination did not cover whole portion of the liver. As the histopathologic processing was performed mainly based on the information provided from USG findings, there is a strong possibility that there were undetected small CCAs or precancerous lesions. As the majority of the detected hepatic masses were confirmed to be CCA, it can be assumed that the precancerous lesions were mainly invisible or indistinguishable on USG. Some of the pathologically unidentified lesions might be precancerous lesions. Thus, to reveal the image findings of the invisible or indistinguishable precancerous lesions, histopathologic full coverage of the liver and thorough retrospective review of image findings with lesion-to-lesion comparison should be mandatory.

Second, follow-up interval of two weeks might be too sparse to detect precancerous lesions. There was no suspected precancerous lesion on retrospective review of USG. One of the possible explanations of this result is too fast change of the precancerous lesions in the CS+NMDA model of

hamsters to detect with two-week interval of follow-up. Thus, closer interval of follow-up will be needed to visualize the chronological change of precancerous lesions to cancerous lesions.

It can be concluded that high-resolution USG and MRI are useful to detect the occurrence of CCAs noninvasively. Although USG was determined not to be a suitable modality in monitoring of the early precancerous lesions of CCA, MRI showed some potential to visualize precancerous lesions of CCAs, but the signal intensity on T2WI was nonspecific to distinguish precancerous lesions from periductal inflammatory change, CCAs, or even dilated intrahepatic bile ducts. MRI of closer interval with more powerful sequences might be able to demonstrate the precancerous lesions of CCAs better.

Acknowledgement

This work was supported by the National Research Foundation of Korea(NRF) grant funded by the Korea government(MSIP) (No. 2009-0083512).

References

1. Jemal, A., et al., *Global patterns of cancer incidence and mortality rates and trends.* Cancer Epidemiol Biomarkers Prev, 2010. **19**(8): p. 1893-907.
2. Shin, H.R., et al., *Descriptive epidemiology of cholangiocarcinoma and clonorchiasis in Korea.* J Korean Med Sci, 2010. **25**(7): p. 1011-6.
3. Lee, J.H., H.J. Rim, and U.B. Bak, *Effect of Clonorchis sinensis infection and dimethylnitrosamine administration on the induction of cholangiocarcinoma in Syrian golden hamsters.* Korean J Parasitol, 1993. **31**(1): p. 21-30.
4. Lee, J.H., et al., *Promoting role of Clonorchis sinensis infection on induction of cholangiocarcinoma during two-step carcinogenesis.* Korean J Parasitol, 1994. **32**(1): p. 13-8.
5. Najm, I. and R.R. Trussell, *NDMA formation in water and wastewater.* Journal American Water Works Association, 2001. **93**(2): p. 92-99.
6. Lee, J.H., H.J. Rim, and S. Sell, *Heterogeneity of the "oval-cell" response in the hamster liver during cholangiocarcinogenesis following Clonorchis sinensis infection and dimethylnitrosamine treatment.* J Hepatol, 1997. **26**(6): p. 1313-23.
7. Plengsuriyakarn, T., et al., *Ultrasonography as a Tool for Monitoring the Development and Progression of Cholangiocarcinoma in Opisthorchis viverrini/Dimethylnitrosamine-Induced Hamsters.* Asian

Pacific Journal of Cancer Prevention, 2012. **13**(1): p. 87-90.

8. Seale, M.K., et al., *Hepatobiliary-specific MR contrast agents: role in imaging the liver and biliary tree.* Radiographics, 2009. **29**(6): p. 1725-48.

9. Choi, D., et al., *Bile duct changes in rats reinfected with Clonorchis sinensis.* Korean J Parasitol, 2004. **42**(1): p. 7-17.

10. Hong, S.T., et al., *Correlation of sonographic findings with histopathological changes of the bile ducts in rabbits infected with Clonorchis sinensis.* Korean J Parasitol, 1994. **32**(4): p. 223-30.

11. Yu, M.H., et al., *Clinical application of controlled aliasing in parallel imaging results in a higher acceleration (CAIPIRINHA)-volumetric interpolated breathhold (VIBE) sequence for gadoxetic acid-enhanced liver MR imaging.* J Magn Reson Imaging, 2013.

12. Kim, K.W., et al., *Free-breathing dynamic contrast-enhanced MRI of the abdomen and chest using a radial gradient echo sequence with K-space weighted image contrast (KWIC).* Eur Radiol, 2013. **23**(5): p. 1352-60.

13. Bock, N.A., et al., *In vivo multiple-mouse MRI at 7 Tesla.* Magnetic Resonance in Medicine, 2005. **54**(5): p. 1311-1316.

14. Hem, A., A.J. Smith, and P. Solberg, *Saphenous vein puncture for blood sampling of the mouse, rat, hamster, gerbil, guinea pig, ferret and mink.* Lab Anim, 1998. **32**(4): p. 364-8.

15. Terpstra, A.H., et al., *A procedure to secure a jugular vein catheter system onto the neck of the hamster.* Lab Anim, 1999. **33**(1): p. 68-70.